ACS APPLIED MATERIALS & INTERFACES

Letter

www.acsami.org

One-Step Synthesis of Amine-Functionalized Hollow Mesoporous Silica Nanoparticles as Efficient Antibacterial and Anticancer Materials

Nanjing Hao, Kalana W. Jayawardana, Xuan Chen, and Mingdi Yan*

Department of Chemistry, University of Massachusetts, Lowell, Massachusetts 01854, United States

Supporting Information

ABSTRACT: In this study, amine-functionalized hollow mesoporous silica nanoparticles with an average diameter of ∼100 nm and shell thickness of ∼20 nm were prepared by an one-step process. This new nanoparticulate system exhibited excellent killing efficiency against mycobacterial (*M. smegmatis* strain mc^2 651) and cancer cells (A549).

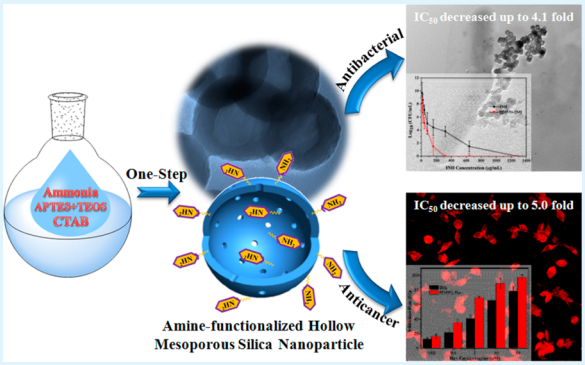

KEYWORDS: *hollow mesoporous silica nanoparticles, amine-functionalized, drug delivery, antibacterial, anticancer*

Mesoporous silica nanomaterials with controlled morphology and structure have attracted increasing attention both for fundamental research on nanointerface and for their widespread potential applications.[1−6] In recent years, much effort has been devoted to the fabrication of mesoporous silica nanoparticles with hollow interiors because of their superior advantages in confined-space catalysis, sustained drug release, renewable energy, and biosensing device.[7−14]

In this regard, several strategies have been developed for constructing hollow mesoporous silica nanoparticles (HMSNs). Among them, the templating methods, including the use of hard templates (such as polystyrene latex particles[15] and hydroxyapatite nanoparticles[16]) and soft templates (such as emulsion droplets[17] and vesicles[18]), are among the most popular. In these cases, the hollow interiors are formed after removing the template either by calcination at high temperature or by selective dissolution in an appropriate solvent. The template-removal process inevitably affects the shell structure, and additionally, the synthetic procedures are time-consuming. Self-templating is another strategy for preparing hollow silica particles. For example, Yin et al. synthesized hollow silica colloids through a spontaneous dissolution-regrowth process from solid silica spheres in alkaline solution with poly(vinylpyrrolidone) as the surface protector.[19,20] Qi and coworkers fabricated gigantic hollow microspheres in mixed water−ethanol solvent using tetraethyl orthosilicate (TEOS) as emulsion droplets.[21] Wang et al. obtained hollow silica particles from solid silica spheres under hydrothermal conditions in acid.[22] However, these strategies either lead to disordered mesoporous channels in the shell, or need further surface modification to introduce reactive functional groups to the materials. Developing simple synthetic protocols that simultaneously give ordered pore channels in the shell and reactive functionalized groups on the surface remains a challenge. Here, we report a simple procedure for the synthesis of amine-functionalized HMSNs from TEOS, 3-aminopropyltriethoxysilane (APTES), and cetyltrimethylammonium bromide (CTAB) in solution phase in a single step. In addition, the new HMSNs were used as efficient drug delivery system for mycobacteria and cells.

HMSNs were prepared by co-condensation of APTES and TEOS in the presence of CTAB as structure directing and pore-forming agent in the shell. A small amount of ammonia was added as the catalyst (see the Supporting Information for details). As shown in Figure 1, nanosized HMSNs were successfully obtained with an average diameter of ca. 100 nm and shell thickness of ca. 20 nm. The dynamic light scattering (DLS) result shows a good dispersion of HMSNs in water with an average hydrodynamic size of 131.7 ± 8.1 nm (see Figure S1 in the Supporting Information). Zeta potential result shows that HMSNs have a high positive potential (+38.09 mV, see Figure S2 in the Supporting Information), which results from the positively charged amino groups on HMSNs. The peaks at 1473, 2865, and 2971 cm^{-1} in the FTIR spectra of HMSNs indicate the presence of organoalkoxysilane in the particles (see Figures S3−S5 in the Supporting Information).[23,24] Thermog-

Received: November 22, 2014
Accepted: January 6, 2015
Published: January 6, 2015

DOI: 10.1021/am508219g
ACS Appl. Mater. Interfaces 2015, 7, 1040−1045

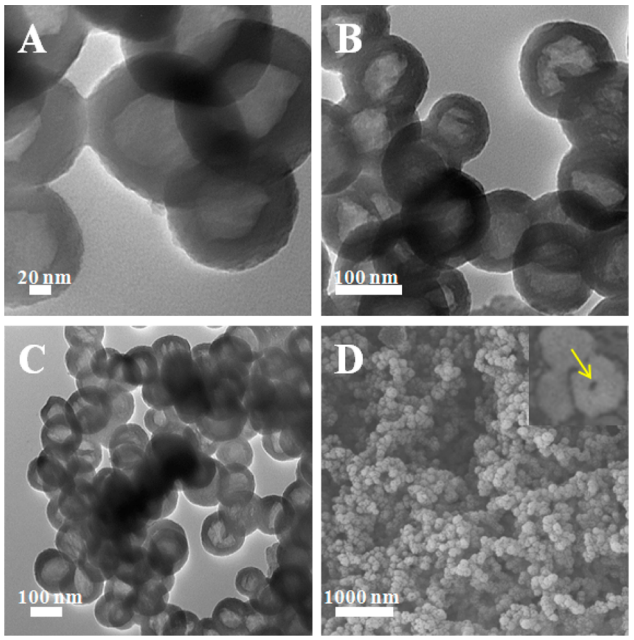

Figure 1. (A–C) TEM images of HMSNs at different magnifications. (D) SEM image of HMSNs. In the inset, the arrow points to a hollow interior of a HMSN.

ravimetric analysis (TGA) results (see Figure S6 in the Supporting Information) showed that HMSNs had a higher weight loss (25.6%) than conventional silica nanoparticles (15.1%) under same treatment conditions due to a relatively high percentage of organic moiety on HSMNs. The surface density of the active amino groups on HMSNs was measured to be about 3.4 amine/nm^2, using the 4-nitrobenzaldehyde assay following a literature protocol.[25] Nitrogen adsorption–desorption measurement shows that HMSNs exhibited a typical type IV isotherm, as expected for HMSNs with ordered cylindrical pores in the shell (see Figure S7A in the Supporting Information).[26] The specific surface area and pore volume of HMSNs were measured to be 410.73 m^2/g and 0.34 cm^3/g, respectively. Note that there was a wide pore size distribution with a sharp peak at 3.1 nm in the HMSNs sample (see Figure S7B in the Supporting Information), which is attributed to its large interior and ordered pore channels have an average pore size of 3.1 nm in the shell layer.

To explore the formation mechanism of HMSNs by this one-step process, we evaluated the specific roles of APTES, CTAB, and the addition order of the reagents (see Figurea S8–10 in the Supporting Information). In the absence of APTES, mesoporous silica nanoparticles of ~40 nm without the hollow structure were obtained (see Figure S8 in the Supporting Information), which indicates that APTES plays a significant role in maintaining the morphology of HMSNs. Without CTAB, the obtained HMSNs aggregated and undefined shell structure was formed (see Figure S9 in the Supporting Information), which suggests that CTAB regulates the shell-forming process. When switching the addition order of reagents, the hollow structure was not observed (see Figure S10 in the Supporting Information), which implies that TEOS and APTES are the determining factors in the formation of the hollow interior. On the basis of these observations, a possible mechanism is proposed to account for the nucleation and growth of HMSNs (Scheme 1). Due to the solubility difference of APTES and TEOS in water (APTES is soluble whereas TEOS is insoluble in water),[27] when they are added to the CTAB solution, the protonated APTES acts as a stabilizer surrounding the TEOS droplets (Scheme 1A, and Figure S8 in the Supporting Information). CTAB micelles could also be captured at the water–oil interface and act as structure-directing agent (Scheme 1B).[21,28] The addition of ammonia initiated and accelerated the hydrolysis of TEOS, and the formed silica fragments that are negatively charged prefer to deposit on the positively charged CTAB micelles. APTES also co-condenses with TEOS to form the shell layer in addition to acting as a morphological stabilizer (Scheme 1C). Because no additional TEOS can be supplied to the oil droplet because of the APTES protecting layer, the condensed materials will form a shell, leading a hollow structure (Scheme 1D). As the reaction progresses, the shell thickness increases until TEOS in the droplet is completely consumed (Scheme 1E).

Scheme 1. Proposed Mechanism for the Formation of HMSNs. (A) Heterogeneous System Consisting of APTES and TEOS in CTAB Aqueous Solution; (B) TEOS Droplets Stabilized by APTES and Captured CTAB micelles; (C) Formation and Deposition of Silica Fragments; (D) Formation of Mesoporous Hollow Structure; (E) Amine-Functionalized Hollow Mesoporous Silica Nanoparticles

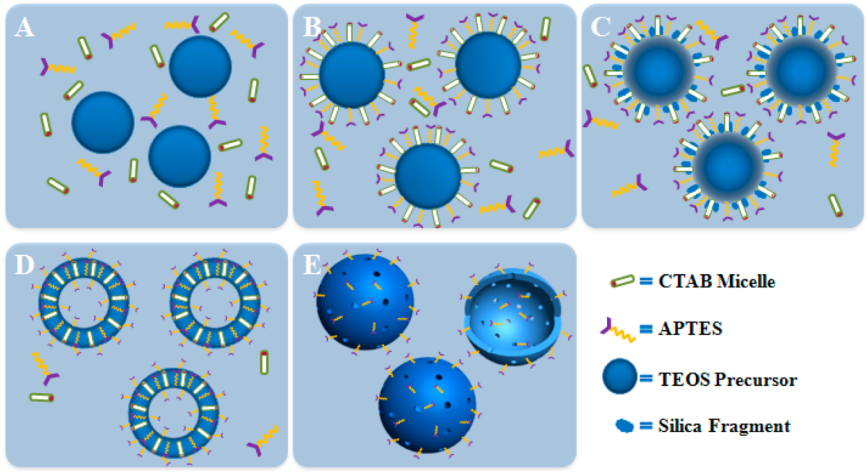

DOI: 10.1021/am508219g
ACS Appl. Mater. Interfaces 2015, 7, 1040–1045

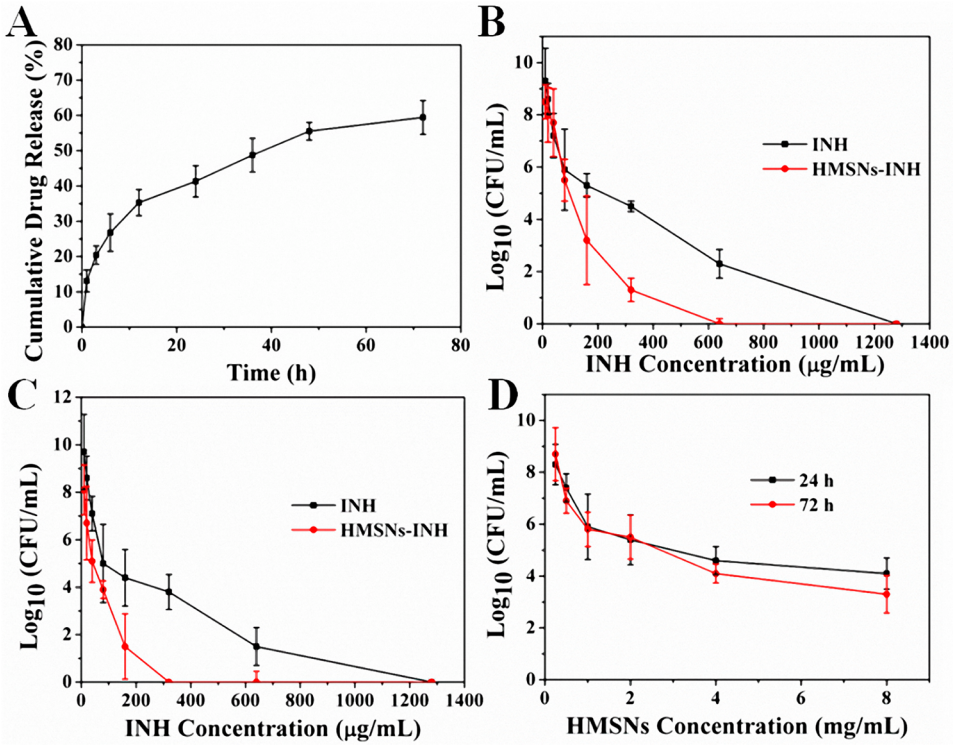

Figure 2. (A) Release profile of INH from drug-loaded HMSNs in PBS solution (pH 6.6); (B, C) Antibacterial efficacy of free INH and INH-loaded HMSNs (concentration of INH from 10 to 1280 μg/mL) on *M. smegmatis* strain mc^2 651 for (B) 24 and (C), 72 h respectively; (D) antibacterial efficacy of HMSNs at a concentration range from 0.25 to 8 mg/mL for 24 and 72 h.

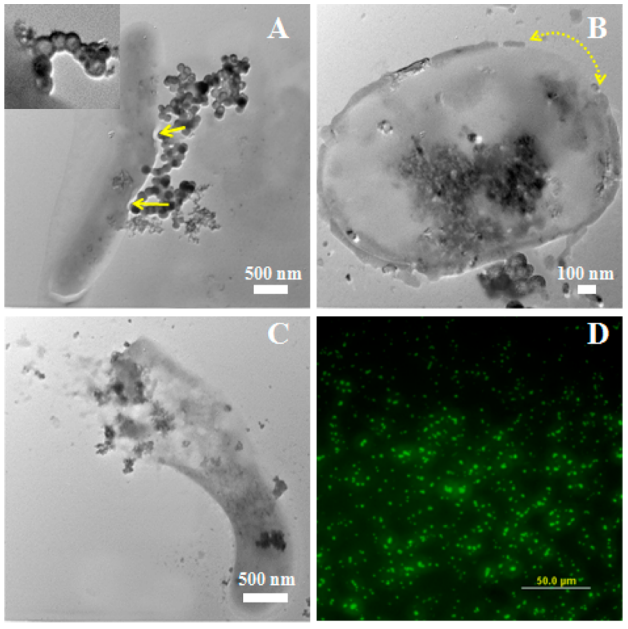

Figure 3. (A–C) TEM images of HMSNs incubated with *M. smegmatis* strain mc^2 651. The inset in A is a magnified image of nanoparticles around bacterium. Arrows in A show bacteria injury, and the arrows in B indicate missing bacteria cell wall. (D) Fluorescence image of *M. smegmatis* strain mc^2 651 treated with HMSNs-FITC.

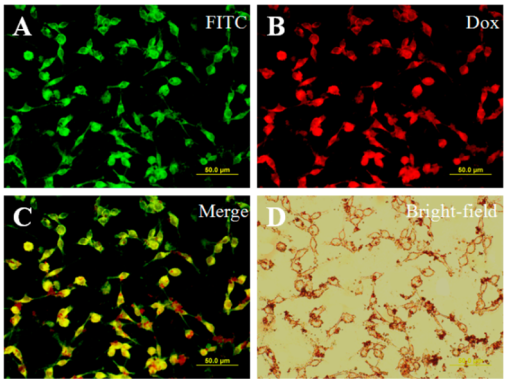

Figure 4. (A–C) Fluorescence and (D) bright-field images of A549 cells after treating with Dox-loaded FITC-labeled HMSNs for 4 h: (A) FITC channel; (B) doxorubicin channel; (C) merged FITC and doxorubicin channels. Scale bars: 50 μm.

These HMSNs have abundant amino groups for further functionalization, large hollow interior that can be used as a reservoir, and a well-defined mesoporous shell that could act as accessible channels for the reagents to diffuse in and out of the interior. Herein, we explore the application of HMSNs as drug delivery vehicle in killing bacteria and cancer cells. Isoniazid (INH), an antituberculosis drug,[29] was loaded into HMSNs. The loading capacity could achieve 315.8 mg per gram of HMSNs (see Figure S11 in the Supporting Information). Figure 2A shows the release profile of INH from INH-loaded HMSNs (HMSNs-INH) in pH 6.6 PBS (simulating the environment of 7H9 broth medium[30]). It can be seen that INH displayed a sustained release profile from HMSNs, and the drug release reached ~60% after 72 h. Mycobacteria-killing kinetics were studied by treating INH-resistant *M. smegmatis* strain mc^2 651 with different concentrations of free INH and INH-loaded HMSNs (INH drug concentration from 10 to 1280 μg/mL) over 24 h (Figure 2B) and 72 h (Figure 2C), and a dose–response relationship was observed. Free INH-treated mycobacteria were completely inhibited at the concentration of

DOI: 10.1021/am508219g
ACS Appl. Mater. Interfaces 2015, 7, 1040–1045

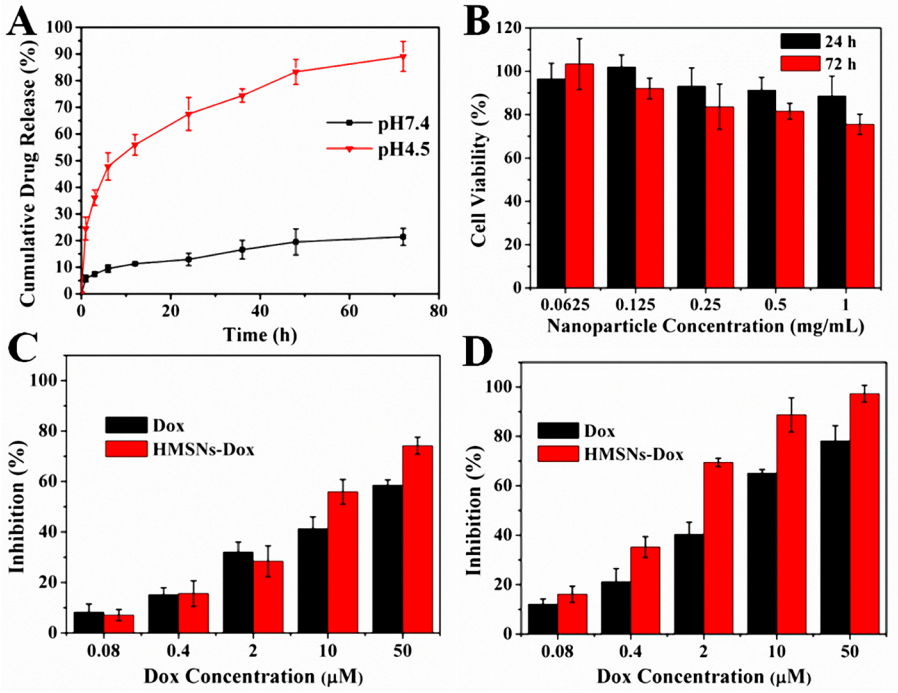

Figure 5. (A) Release profile of Dox from HMSNs-Dox in PBS buffer (pH 4.5 and pH 7.4); (B) A549 cell viability with concentrations of HMSNs from 0.0625 to 1 mg/mL for 24 and 72 h. (C, D) Inhibition rates of Dox and HMSNs-Dox (at concentration of Dox from 0.08 to 50 μM) on A549 cells for 24 and 72 h, respectively.

1280 μg/mL for both 24 and 72 h incubation, while HMSNs-INH-treated mycobacteria were completely inhibited at the concentration of 640 and 320 μg/mL for 24 and 72 h incubation, respectively. In addition, the half inhibitory concentration (IC_{50}) of mycobacteria treated by free INH drug was 3.3- and 4.1-fold of HMSNs-INH-treated bacteria at 24 and 72 h, respectively. This enhanced antibacterial activity might be probably due to increased intrabacterial accumulation of sustained INH drugs from HMSNs-INH and partly by the strong interactions between HMSNs and bacteria.[29] HMSNs alone had bacteria-killing effect to some extent, especially at high particle concentrations of >1 mg/mL (Figure 2D). This is anticipated since quaternary ammonium species are known to have antimicrobial activities.[31,32]

We next investigated the interactions between HMSNs and mycobacteria. As shown in Figure 3, HMSNs could efficiently bind to the bacteria surface likely due to the nonspecific adsorption of the positively charged amine-nanoparticles onto the negatively charged bacteria cell surface.[33] Further examination of the images revealed that the interactions of HMSNs also led to bacteria injury (Figure 3A), incomplete or missing bacteria cell wall (Figure 3B), and even bacteria rupture and death (Figure 3C), which is consistent with the results in Figure 2D. This is in clear contrast to the negatively charged conventional mesoporous silica nanoparticles (see Figure S12 in the Supporting Information) which had minimal interactions with mycobacteria (see Figure S13 in the Supporting Information). The strong interaction between HMSNs and bacteria was also confirmed using FITC-labeled HMSNs fluorescent nanoparticles, where the mycobacteria became fluorescent after treating with HMSNs-FITC (Figure 3D and Figures S14 and S15 in the Supportng Information). These preliminary results demonstrated that HMSNs has the potential to be used as an effective nanovehicle for treating drug-resistant bacteria.

To further explore the potential of HMSNs, we loaded anticancer drug doxorubicin (Dox) into HMSNs, and its efficacy toward A549 cells was evaluated. After treating the Dox-loaded HMSNs-FITC, the particles were efficiently internalized into A549 cells (Figure 4 and Figure S16 in the Supporting Information). The loading capacity of Dox was 261.5 mg per gram of nanoparticles (see Figure S17 in the Supporting Information). The sustained release profiles of Dox from Dox-loaded HMSNs (HMSNs-Dox) were measured in pH 7.4 and pH 4.5 PBS to simulate the environment of extracellular incubating medium and intracellular endosomal-lysosomal acidification, respectively.[34] The cumulative drug release were 21.4 and 89.1% after 72 h in pH 7.4 and pH 4.5 PBS, respectively (Figure 5A). Cell viability test using A549 cells shows no significant adverse effect even at high HMSNs particle concentration of 1 mg/mL (Figure 5B). When A549 cells were incubated with a series of equivalent drug concentrations of free Dox and HMSNs-Dox for 24 and 72 h, both free Dox and HMSNs-Dox shows obvious cell inhibition after 24 h (Figure 5C) and 72 h incubation (Figure 5D) with Dox concentration from 0.08 to 50 μM. However, the IC_{50} values of Dox are 3.9- and 5.0-fold of HMSNs-Dox at 24 h (31.6 μM for Dox and 8.1 μM for HMSNs-Dox) and 72 h (5.5 μM for Dox and 1.1 μM for HMSNs-Dox) respectively. The increased cytotoxicity of HMSNs-Dox can be attributed to the sustained release of Dox from HMSNs-Dox, and perhaps to the enhanced Dox uptake by A549 cells when Dox encapsulated into amine-enriched HMSNs.[35]

In summary, we have successfully developed a one-step strategy to synthesize amine-functionalized HMSNs with well-defined mesoporous shell. When loaded with an antibiotic or a cancer drug, these HMSNs exhibited excellent antibacterial (*M. smegmatis* strain mc^2 651) and anticancer (A549) activities lowering the IC_{50} values by several folds. The increased activities can be attributed to its unique structures including the

DOI: 10.1021/am508219g
ACS Appl. Mater. Interfaces 2015, 7, 1040−1045

amine surface for enhanced interactions with cells, large hollow interior cavity as drug reservoir, and well-defined mesoporous shell for sustained drug release. This general synthetic strategy can be extended to fabricate hollow nanomaterials of different structure and shape, paving the way for the applications of these nanomaterials in many fields such as catalysis, adsorption, separation, and microreactors.

■ ASSOCIATED CONTENT

Ⓢ Supporting Information

Experimental details, materials characterization and additional data. This material is available free of charge via the Internet at http://pubs.acs.org.

■ AUTHOR INFORMATION

Corresponding Author

*E-mail: mingdi_yan@uml.edu. Fax: +1-978-334-3013. Tel: +1-978-334-3647.

Notes

The authors declare no competing financial interest.

■ ACKNOWLEDGMENTS

The authors thank the financial support of this work from the National Institutes of Health (R01GM080295, R21AI109896), and a startup grant from University of Massachusetts Lowell. We thank Professor William R. Jacobs of Albert Einstein College of Medicine for the kind gift of mycobacteria.

■ REFERENCES

(1) Geng, Y.; Dalhaimer, P.; Cai, S. S.; Tsai, R.; Tewari, M.; Minko, T.; Discher, D. E. Shape Effects of Filaments versus Spherical Particles in Flow and Drug Delivery. *Nat. Nanotechnol.* **2007**, *2*, 249−255.

(2) Yang, P. P.; Gai, S. L.; Lin, J. Functionalized Mesoporous Silica Materials for Controlled Drug Delivery. *Chem. Soc. Rev.* **2012**, *41*, 3679−3698.

(3) Yang, K.; Ma, Y. Q. Computer Simulation of the Translocation of Nanoparticles with Different Shapes across a Lipid Bilayer. *Nat. Nanotechnol.* **2010**, *5*, 579−583.

(4) Hao, N. J.; Li, L. F.; Tang, F. Q. Shape-Mediated Biological Effects of Mesoporous Silica Nanoparticles. *J. Biomed. Nanotechnol.* **2014**, *10*, 2508−2538.

(5) Hao, N. J.; Li, L. F.; Tang, F. Q. Facile Preparation of Ellipsoid-like MCM-41 with Parallel Channels along the Short Axis for Drug Delivery and Assembly of Ag Nanoparticles for Catalysis. *J. Mater. Chem. A* **2014**, *2*, 11565−11568.

(6) Hao, N. J.; Yang, H. H.; Li, L. F.; Li, L. L.; Tang, F. Q. The Shape Effect of Mesoporous Silica Nanoparticles on Intracellular Reactive Oxygen Species in A375 Cells. *New J. Chem.* **2014**, *38*, 4258−4266.

(7) Liu, J.; Qiao, S. Z.; Chen, J. S.; Lou, X. W.; Xing, X. R.; Lu, G. Q. Yolk/shell Nanoparticles: New Platforms for Nanoreactors, Drug Delivery and Lithium-Ion Batteries. *Chem. Commun.* **2011**, *47*, 12578−12591.

(8) Tsou, C. J.; Chu, C. Y.; Hung, Y.; Mou, C. Y. A Broad Range Fluorescent pH Sensor Based on Hollow Mesoporous Silica Nanoparticles, Utilising the Surface Curvature Effect. *J. Mater. Chem. B* **2013**, *1*, 5557−5563.

(9) Lou, X. W. (David); Archer, L. A.; Yang, Z. C. Hollow Micro-/Nanostructures: Synthesis and Applications. *Adv. Mater.* **2008**, *20*, 3987−4019.

(10) Du, X.; He, J. H. Spherical Silica Micro/nanomaterials with Hierarchical Structures: Synthesis and Applications. *Nanoscale* **2011**, *3*, 3984−4002.

(11) Tang, F. Q.; Li, L. L.; Chen, D. Mesoporous Silica Nanoparticles: Synthesis, Biocompatibility and Drug Delivery. *Adv. Mater.* **2012**, *24*, 1504−1534.

(12) Chen, Y.; Meng, Q. S.; Wu, M. Y.; Wang, S. G.; Xu, P. F.; Chen, H. R.; Li, Y. P.; Zhang, L. X.; Wang, L. Z.; Shi, J. L. Hollow Mesoporous Organosilica Nanoparticles: A Generic Intelligent Framework-Hybridization Approach for Biomedicine. *J. Am. Chem. Soc.* **2014**, *136*, 16326−16334.

(13) Zhang, J.; Karmakar, S.; Yu, M. H.; Mitter, N.; Zou, J.; Yu, C. Z. Synthesis of Silica Vesicles with Controlled Entrance Size for High Loading, Sustained Release, and Cellular Delivery of Therapeutical Proteins. *Small* **2014**, DOI: 10.1002/smll.201401538.

(14) Jiao, Y. F.; Guo, J.; Shen, S.; Chang, B. S.; Zhang, Y. H.; Jiang, X. G.; Yang, W. L. Synthesis of Discrete and Dispersible Hollow Mesoporous Silica Nanoparticles with Tailored Shell Thickness for Controlled Drug Release. *J. Mater. Chem.* **2012**, *22*, 17636−17643.

(15) Kato, N.; Ishii, T.; Koumoto, S. Z. Synthesis of Monodisperse Mesoporous Silica Hollow Microcapsules and Their Release of Loaded Materials. *Langmuir* **2010**, *26*, 14334−14344.

(16) Williamson, P. A.; Blower, P. J.; Green, M. A. Synthesis of Porous Hollow Silica Nanostructures Using Hydroxyapatite Nanoparticle Templates. *Chem. Commun.* **2011**, *47*, 1568−1570.

(17) Lin, Y. S.; Wu, S. H.; Tseng, C. T.; Hung, Y.; Chang, C.; Mou, C. Y. Synthesis of Hollow Silica Nanospheres with a Microemulsion as the Template. *Chem. Commun.* **2009**, *24*, 3542−3544.

(18) Wu, X. J.; Xu, D. S. Formation of Yolk/SiO(2) Shell Structures Using Surfactant Mixtures as Template. *J. Am. Chem. Soc.* **2009**, *131*, 2774−2775.

(19) Zhang, T. R.; Ge, J. P.; Hu, Y. X.; Zhang, Q.; Aloni, S.; Yin, Y. D. Formation of Hollow Silica Colloids through a Spontaneous Dissolution-Regrowth Process. *Angew. Chem., Int. Ed.* **2008**, *47*, 5806−5811.

(20) Zhang, Q.; Zhang, T. R.; Ge, J. P.; Yin, Y. D. Permeable Silica Shell through Surface-Protected Etching. *Nano Lett.* **2008**, *8*, 2867−2871.

(21) Zhang, H. J.; Wu, J.; Zhou, L. P.; Zhang, D. Y.; Qi, L. M. Facile Synthesis of Monodisperse Microspheres and Gigantic Hollow Shells of Mesoporous Silica in Mixed Water-Ethanol Solvents. *Langmuir* **2007**, *23*, 1107−1113.

(22) Yu, Q. Y.; Wang, P. P.; Hu, S.; Hui, J. F.; Zhuang, J.; Wang, X. Hydrothermal Synthesis of Hollow Silica Spheres under Acidic Conditions. *Langmuir* **2011**, *27*, 7185−7191.

(23) Hao, N. J.; Li, L. L.; Zhang, Q.; Huang, X. L.; Meng, X. W.; Zhang, Y. Q.; Chen, D.; Tang, F. Q.; Li, L. F. The Shape Effect of PEGylated Mesoporous Silica Nanoparticles on Cellular Uptake Pathway in Hela Cells. *Microporous Mesoporous Mater.* **2012**, *162*, 14−23.

(24) Hao, N. J.; Liu, H. Y.; Li, L. L.; Chen, D.; Li, L. F.; Tang, F. Q. In Vitro Degradation Behavior of Silica Nanoparticles Under Physiological Conditions. *J. Nanosci. Nanotechnol.* **2012**, *12*, 6346−6354.

(25) Moon, J. H.; Kim, J. H.; Kim, K.; Kang, T. H.; Kim, B.; Kim, C. H.; Hahn, J. H.; Park, J. W. Absolute Surface Density of the Amine Group of the Aminosilylated Thin Layers: Ultraviolet-Visible Spectroscopy, Second Harmonic Generation, and Synchrotron-Radiation Photoelectron Spectroscopy Study. *Langmuir* **1997**, *13*, 4305−4310.

(26) Sing, K. S. W.; Everett, D. H.; Haul, R. A. W.; Moscou, L.; Pierotti, R. A.; Rouquerol, J.; Siemieniewska, T. Reporting Physisorption Data for Gas/solid Systems with Special Reference to the Determination of Surface Area and Porosity. *Pure Appl. Chem.* **1985**, *57*, 603−619.

(27) Yang, X. L.; Zhao, N.; Zhou, Q. Z.; Wang, Z.; Duan, C. T.; Cai, C.; Zhang, X. L.; Xu, J. Facile Preparation of Hollow Amino-Functionalized Organosilica Microspheres by a Template-Free Method. *J. Mater. Chem.* **2012**, *22*, 18010−18017.

(28) Tan, L. F.; Liu, T. L.; Li, L. L.; Liu, H. Y.; Wu, X. L.; Gao, F. P.; He, X. L.; Meng, X. W.; Chen, D.; Tang, F. Q. Uniform Double-Shelled Silica Hollow Spheres: Acid/base Selective-Etching Synthesis and Their Drug Delivery Application. *RSC Adv.* **2013**, *3*, 5649−5655.

(29) Clemens, D. L.; Lee, B. Y.; Xue, M.; Thomas, C. R.; Meng, H.; Ferris, D.; Nel, A. E.; Zink, J. I.; Horwitz, M. A. Targeted Intracellular Delivery of Antituberculosis Drugs to Mycobacterium Tuberculosis-

DOI: 10.1021/am508219g
ACS Appl. Mater. Interfaces 2015, 7, 1040−1045

Infected Macrophages via Functionalized Mesoporous Silica Nanoparticles. *Antimicrob. Agents Chemother.* **2012**, *56*, 2535−2545.
(30) Carlson, L. D. C.; Wallis, C. K.; Coyle, M. B.; Carlson, L. A. D. C. Standardized BACTEC Method To Measure Clarithromycin Susceptibility of Mycobacterium Genavense Standardized BACTEC Method To Measure Clarithromycin Susceptibility of Mycobacterium Genavense. *J. Clin. Microbiol.* **1998**, *36*, 748−751.
(31) Beyth, N.; Yudovin-Farber, I.; Bahir, R.; Domb, A. J.; Weiss, E. I. Antibacterial Activity of Dental Composites Containing Quaternary Ammonium Polyethylenimine Nanoparticles against Streptococcus Mutans. *Biomaterials* **2006**, *27*, 3995−4002.
(32) Jia, Z. S.; Shen, D. F.; Xu, W. L. Synthesis and Antibacterial Activities of Quaternary Ammonium Salt of Chitosan. *Carbohydr. Res.* **2001**, *333*, 1−6.
(33) Dickson, J. S.; Koohmaraie, M. Cell Surface Charge Characteristics and Their Relationship to Bacterial Attachment to Meat Surfaces. *Appl. Environ. Microbiol.* **1989**, *55*, 832−836.
(34) Varkouhi, A. K.; Scholte, M.; Storm, G.; Haisma, H. J. Endosomal Escape Pathways for Delivery of Biologicals. *J. Controlled Release* **2011**, *151*, 220−228.
(35) Slowing, I. I.; Trewyn, B. G.; Lin, V. S.-Y. Effect of Surface Functionalization of MCM-41-Type Mesoporous Silica Nanoparticles on the Endocytosis by Human Cancer Cells. *J. Am. Chem. Soc.* **2006**, *128*, 14792−14793.

DOI: 10.1021/am508219g
ACS Appl. Mater. Interfaces 2015, 7, 1040−1045